GEOLOGIJA *60/2*, 199–210, Ljubljana 2017
https://doi.org/10.5474/geologija.2017.014

Analysis of systematic fracturing in Eocene flysch of the Slovenian coastal region

Analiza sistematične razpokanosti eocenskih flišnih kamnin Slovenske obale

Marko VRABEC & Galena JORDANOVA

Univerza v Ljubljani, Naravoslovnotehniška fakulteta, Oddelek za geologijo,
Privoz 11, SI –1000 Ljubljana, Slovenija; e-mail: marko.vrabec@geo.ntf.uni-lj.si

Prejeto / Received 1. 3. 2017; Sprejeto / Accepted 10. 10. 2017; Objavljeno na spletu / Published online 22. 12. 2017

Dedicated to Professor France Šušteršič on the occasion of his 70th birthday

Key words: Eocene flysch, systematic fractures, paleostress, joints, fracture spacing index, Istria, Slovenia
Ključne besede: Eocenski fliš, sistematične razpoke, paleonapetosti, natezne razpoke, indeks oddaljenosti razpok, Istra, Slovenija

Abstract

We analyse systematic fractures occurring in sandstone beds in Eocene flysch of the Slovenian coastal area. Two nearly perpendicular fracture sets were identified: fractures F1 are generally NW-SE oriented, well-expressed and predominately planar, whereas fractures F2 are NE-SW-striking, shorter, more irregular in shape, and terminate against the F1 set. The average orientation of both sets does not change significantly in a coastal transect crossing all principal structural domains of the area. We analysed fracture spacing with respect to layer thickness and determined fracture spacing index for both fracture sets. We interpret both fracture sets as tensional (Mode I) joints originating in two distinct extensional episodes. Set F1 is older and formed in NE-SW directed tension which we correlate with the well-documented regional post-Dinaric orogen-perpendicular extension of presumably mid-Miocene age. Set F2 formed in NW-SE oriented tension, which is compatible with previously documented NE-SW-striking normal faults occurring in the area, but was so far not documented elsewhere. We interpret that F1 fractures predate folding and thrusting in the coastal belt. Earlier, Eocene-Oligocene Dinaric thrusting therefore did not significantly affect the coastal area, whereas post-F1 shortening, associated with northward indentation and underthrusting of the Adria microplate, did not commence before late Miocene.

Izvleček

Raziskali smo sistematične razpoke, ki se pojavljajo v plasteh peščenjaka v eocenskem flišu Slovenske obale. Pojavljata se dve, medsebojno skoraj pravokotni družini razpok: razpoke družine F1 so generalno usmerjene v SZ-JV smeri in so dobro izražene in pretežno planarne, razpoke družine F2 pa imajo smer SV-JZ in so krajše, bolj nepravilno oblikovane in se zaključujejo na ploskvah razpok F1. Povprečna orientacija razpok obeh družin se bistveno ne spreminja vzdolž raziskanega profila, ki preči vse glavne strukturne domene ob Obali. Analizirali smo medsebojno oddaljenost razpok glede na debelino plasti in obema družinama določili indeks oddaljenosti razpok (fracture spacing index). Obe družini interpretiramo kot natezne razpoke tipa I, ki so nastale v dveh ločenih fazah natezne tektonike. Družina F1 je starejša in je nastala v SV-JZ usmerjeni tenziji in jo povezujemo z dobro poznano regionalno fazo post-Dinarske ekstenzije, ki je domnevno srednje miocenske starosti. Družina F2 je nastala v SZ-JV usmerjeni tenziji in je skladna z SV-JZ usmerjenimi normalnimi prelomi, ki so bili že prej dokumentirani v območju Obale, ni pa še bila odkrita v ostalih delih Slovenije. Po naši interpretaciji so razpoke družine F1 starejše od narivanja in gubanja v območju Obale. Zato sklepamo, da predhodno Dinarsko narivanje eocensko-oligocenske starosti ni bistveno prizadelo obalnega območja. Krčenje ozemlja po nastanku razpok F1, ki ga povezujemo s podrivanjem Jadranske mikroplošče proti severu, pa se ni začelo pred mlajšim miocenom.

Introduction

The territory of Slovenia was affected by polyphase tectonic deformation (e.g. Vrabec et al. 2009 and references therein), which not only produced a complex regional assemblage of tectonic units (Placer, 2008), but is also reflected in outcrop-scale structural geometry. It is therefore rarely possible to observe structurally homogeneous systematic sets of structures. One such exception occurs in the coastal region of Slovenia, which structurally represents the most external part of the Dinaric fold-and-thrust belt. Here, the generally flat-lying to gently-dipping beds of Eocene flysch nearly everywhere have pervasive systematic fractures. We present a first structural analysis of these fracture sets with the aim to examine their geometry, to interpret their origin and tectonic significance, and to investigate whether meaningful statistical properties, specifically the fracture spacing index (FSI), can be derived to characterize the fracture sets. These data are useful not only for understanding the tectonic evolution of the area, but may also be relevant for various applications such as in hydrogeology, engineering geology, and in geothermal resources development.

Geological setting

The coastal region of Slovenia, geographically situated in northwestern part of the Istria penninsula (Fig. 1), sits in the Adriatic – Apulian foreland of the fold-and-thrust belt of the northwestern External Dinarides (Placer, 2008; Placer et al., 2010). The coastal area was affected by two major Tertiary shortening episodes: the Eocene-Oligocene SW-directed thrusting of the External Dinarides, and the subsequent underthrusting of the Adriatic microplate below the Dinarides and the Southern Alps, which is at present time NNW-directed (e.g. Weber et al, 2010).

Major stratigraphic units of the area comprise Mesozoic – Palaeocene carbonates of the Adriatic carbonate platform, which are uncomfortably overlain by Eocene turbidites (flysch) deposited in SW-ward migrating foreland basin in front of the advancing Dinaric orogen (Otoničar, 2007). Flysch in the Slovenian coastal area is of distal facies where well-bedded predominately cm-dm thick siliciclastic sandstones are interbedded with marls in approximately equal proportion (Pavšič & Peckmann, 1996). This monotonous sequence is interrupted by a number of distinct 1 – 5 m thick calciturbiditic horizons, derived from the carbonate platform which persisted in front of the foreland basin throughout Eocene (Pavšič & Peckmann, 1996; Placer et al. 2004, Vrabec & Rožič, 2014). In the offshore in the Gulf of Trieste, a several hundred m thick succession of Pliocene to Quaternary continental and marine sediments is covering the flysch sequence, with the topmost sedimentary cover represented by up to ten m of Holocene marine clay (Busetti et al., 2010).

The transition from the inland karstic plateau of Kras where Mesozoic carbonate rocks prevail to the coastal lowland area dominated by Eocene flysch siliciclastics is structurally and morphologically defined by the NW-SE-striking Palmanova Thrust System (Fig. 1), comprising several sub-parallel thrust faults with various local names, spanning from Palmanova in Italy to Mt. Učka in Croatia (Placer, 2008, Carulli, 2011). A vertical displacement component of approx. 1000 m is inferred on this thrust system, hence the name Dinaric Frontal Ramp was also proposed (e.g. Busetti et al., 2010). External to this thrust boundary, between the Bay of Milje (Muggia) and Bay of Koper, careful structural mapping has revealed a series of low-angle thrust faults with km-scale displacements, cutting the Eocene flysch and locally producing vertical or even inverted

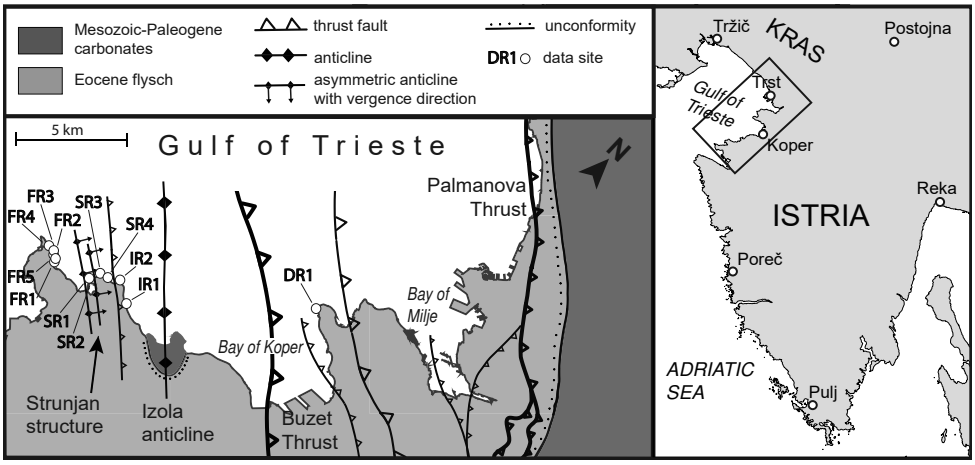

Fig. 1. Structural map of the investigated area with locations of measurement sites (simplified from Placer, 2007, Vrabec et al., 2014 & Placer, 2015).

bedding (Placer, 2007). Of those, the prominent Buzet Thrust, reaching the coastline at Koper, was inferred to have a displacement in excess of 10 km (Placer et al. 2004; Placer, 2007) and can be traced on marine seismic reflection profiles towards the middle of the Gulf of Trieste (Vrabec et al., 2014). The considerable amount of shortening deformation and the generally low-angle geometry of these structures led Placer (2007) to interpret them as reflecting a younger phase of convergence related to Adria underthrusting and not as the frontal imbricate structures of the Dinaric thrust system, as previously believed.

Further southwest of the Buzet Thrust, the degree of deformation is much lower. Here, the strata are gently folded forming the Izola Anticline with Paleocene carbonates outcropping in the fold core near the town of Izola (Fig.1). The most external deformation observed along the Slovenian coastline occurs at Strunjan, where several NE-verging reverse faults and asymmetric folds disrupt the flysch sequence (Strunjan structure of Placer, 2005). Still further southwest, from Fiesa to Piran, the beds are essentially undeformed and nearly flat-lying.

At least two extensional episodes were also documented in the region. First is a NE-SW oriented extension postdating the Dinaric thrusting and occurring everywhere along the Dinarides. This extension is probably concurrent with mid-Miocene extension and basin subsidence in the Pannonian domain (Vrabec & Fodor, 2006; Žibret & Vrabec, 2016). A second episode, documented so far only in the coastal area, exhibits NW-SE-oriented tension, which is manifested in normal faults with NE-SW strike, occurring both in map-scale (Placer, 2005) and in outcrop-scale (Vrabec & Rožič, 2014).

The youngest tectonic phase documented in the region is the ongoing NNW-SSE directed compression, which probably started in Pliocene (Vrabec & Fodor, 2006; Weber et al., 2010; see also Moulin et al., 2016). This phase is mainly manifested by dextral slip on NW-SE-striking faults (Žibret & Vrabec, 2016), which however are not common in the Slovenian coastal area.

Methods

We collected fracture data at 12 sites spanning all principal structural domains of the coastal region (Fig. 1): the low-angle thrust system between the Palmanova Thrust and Buzet Thrust (site DR1), the southern limb of the Izola Anticline (sites IR1 and IR2), the Strunjan structure (sites SR1 to SR4), and the undeformed foreland (sites FR1 to FR5). A list of sites with their coordinates is presented in Table 1. At each site, we measured fractures in several sandstone beds of different thickness to provide representative bed thickness / fracture density data. We were primarily choosing beds with good 3D exposure to maximize measurement quality.

Orientations of bedding planes and fractures were measured with digital geological compass GeoClino Digital Clinometer, which provides fast and reliable measuring procedure, and conveniently facilitates data storage into internal memory. To ensure measurement precision, digital compass was carefully calibrated according to manufacturer instructions at each measurement site. For additional control, digital readouts were checked several times against measurements with classical Freiberg-style geological compass.

Fracture spacing and bed thickness was measured with ordinary measuring tape. Fracture spacing was measured perpendicular to fracture strike. Sections of the outcrops with well-developed straight and parallel fracture traces were exclusively considered for measuring.

Orientation data were processed and analysed with Orient software, version 2.1.2.2 (Vollmer, 2015). Software utility GeoCalculator version 4.9.8 written by Rob Holcombe was used to calculate intersecting angles between fracture sets. Fractures were separately analysed on a per-bed, per-site and per-domain basis.

Structural analysis

Strata at investigated sites predominately dip gently to the SSW (Table 1; Fig. 4a). Dip angles mostly range between 10° and 15°, except in the most external part of the study area (sites FR), where bedding is nearly flat-lying. At all investigated sites, systematic fractures predominately occur in thick (decimetre-scale) sandstone beds as planar to moderately curviplanar planes (Fig. 2). Only occasionally fractures exhibit more irregular configurations resembling polygonal structure, but such configurations appear to be limited to certain beds, whereas adjacent beds above and below in the stratigraphic succession normally have more regular fracture geometry.

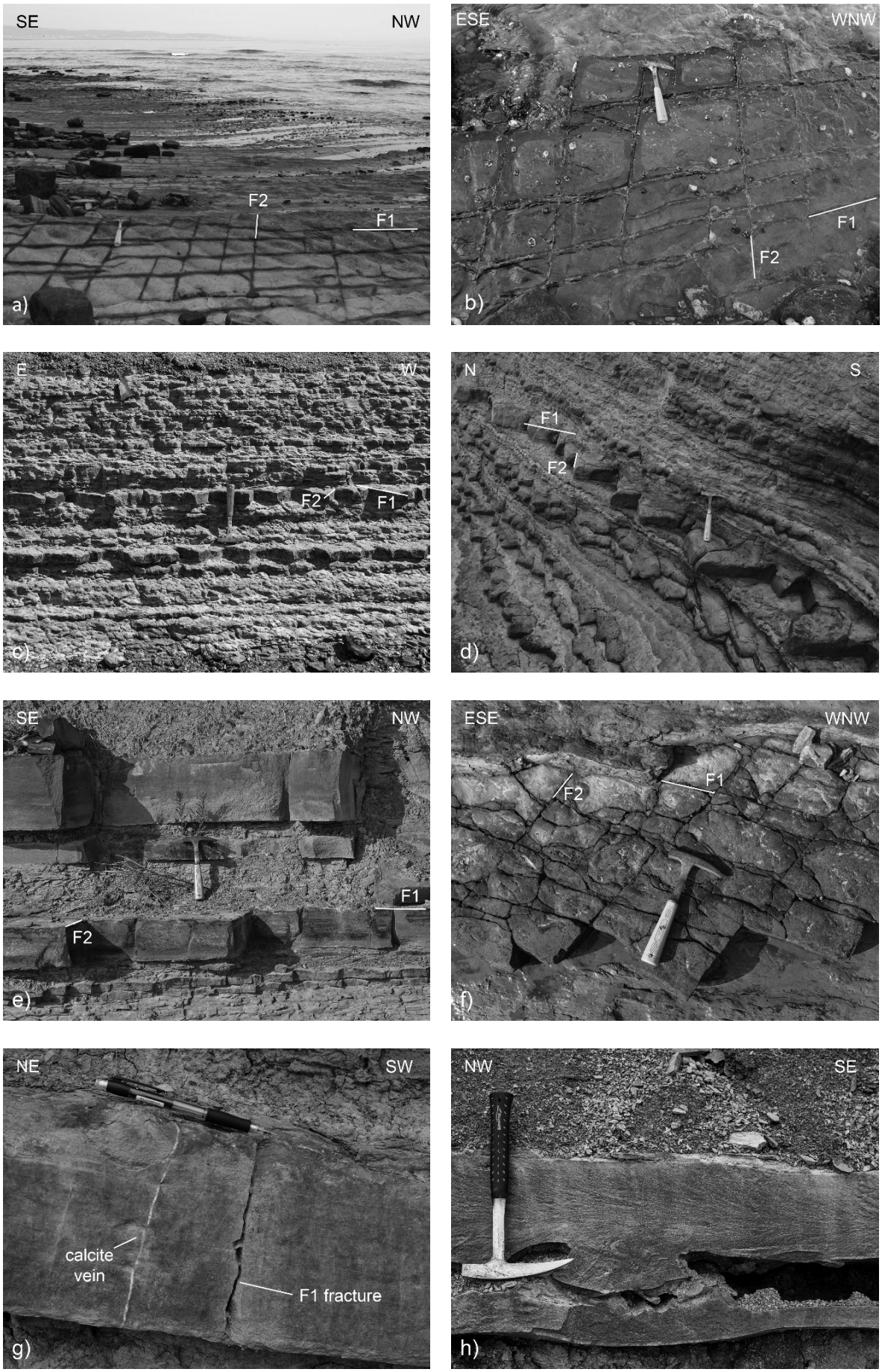

Fig. 2. Typical outcrop examples of investigated systematic fractures in Eocene flysch. a) and b) Debeli rtič (site DR1). c) Bele skale (site IR1). d) Rtič Strunjan (site SR3). e) Fiesa (site FR1). f) Fiesa (site FR2). g) Calcite-filled tension gash parallel to F1 fracture planes, Strunjan (close to Site SR1). h) Plumose ornamentations on F1 fracture plane, indicating horizontal (Mode I) propagation directed from right to left, Rt Ronek (between sites SR4 and IR2).

Systematic fractures appear in two well-defined sets, which we name F1 and F2 (Table 1; Figs. 2, 3, 4). The NW-SE-striking F1 fractures are normally longer with more straight traces. The generally NE-SW-trending F2 fractures are shorter and mainly appear to terminate against F1 set, although this relationship between the two sets is not everywhere clear. F2 fractures are also more curviplanar and irregular in orientation. This is reflected in orientation distributions (Fig. 3), where F2 fractures show considerably greater spread of orientations compared to F1 fractures. The angle of intersection between the two sets is quite constant at around 80° on the average, but ranges from 65° to nearly perpendicular (Table 1).

The NW-SE orientation of F1 fractures is relatively stationary between the sites and in all structural domains investigated in the study, with the exception of Strunjan structure (Figs. 3, 4b, 4d). There, a pronounced deviation to WNW-ESE or even E-W orientation is observed. Additionally, a large variation in fracture sets orientation from bed to bed in the same section can be seen (see data for sites SR1 and SR2 in Fig. 2), reflecting perhaps the mechanical influence of intervening soft layers and the varying thickness of the sandstone beds and their interlayers. This was not noted at other sites. Within the Strunjan structure also F2 fracture orientations deviate from their general NE-SW trend towards a more N-S orientation, which is particularly clear at site SR2 (Fig. 2).

Fig. 3. Measured fracture orientations in spherical projection (equal-area projection, lower hemisphere). First column: present-day orientation. Bedding orientation is displayed with thick dark-grey traces. Second column: data backtilted to original (bedding-horizontal) position. Thick black traces indicate the average orientation (medium vector) of each fracture set. Third and fourth column: circular histogram of fracture strike directions (in backtilted orientation) for each fracture set. Bin size is 5°.

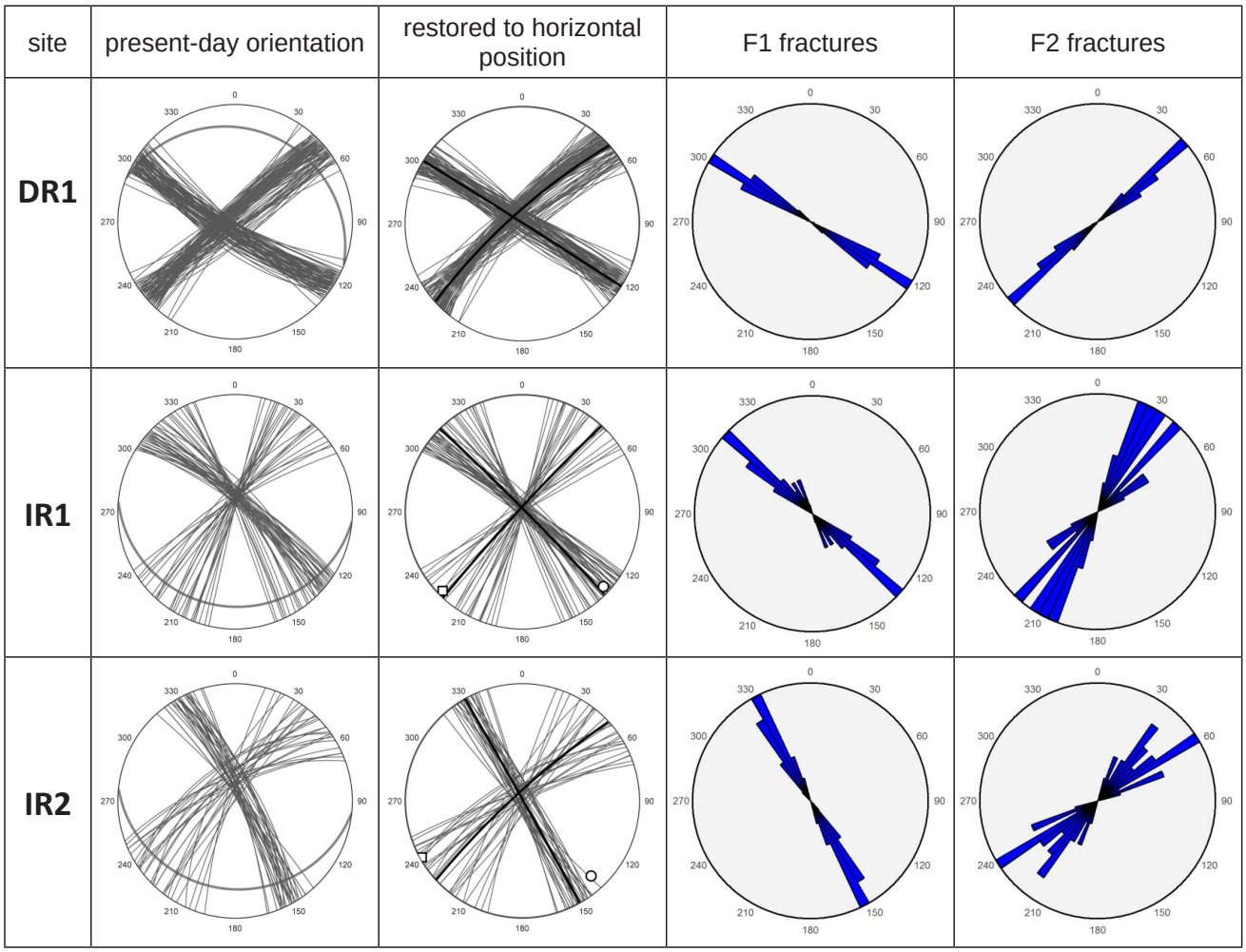

site	present-day orientation	restored to horizontal position	F1 fractures	F2 fractures
SR1 P1	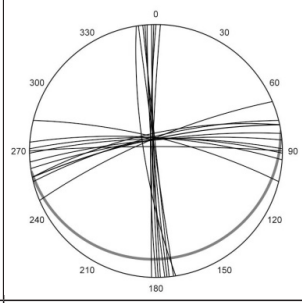	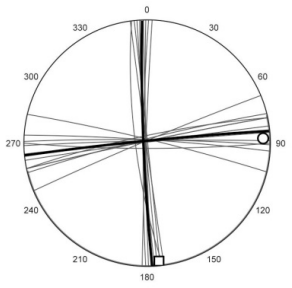	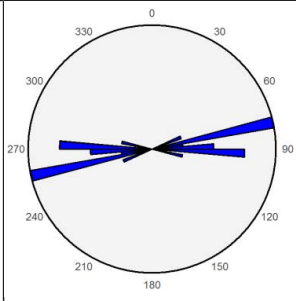	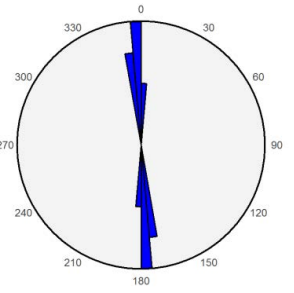
SR1 P2	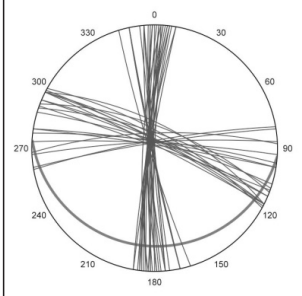	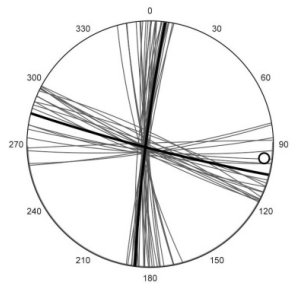	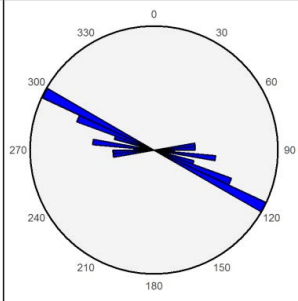	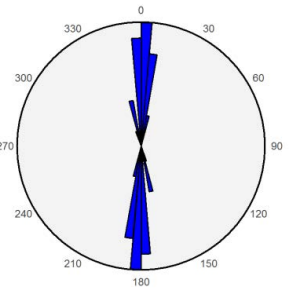
SR1 P3	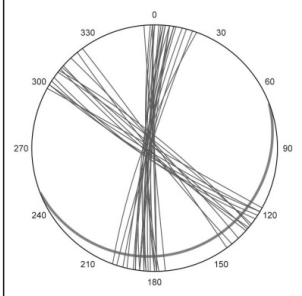	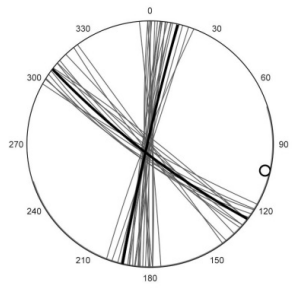	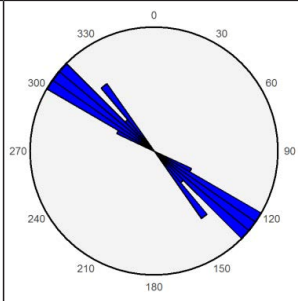	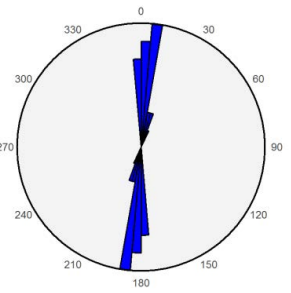
SR2 P1	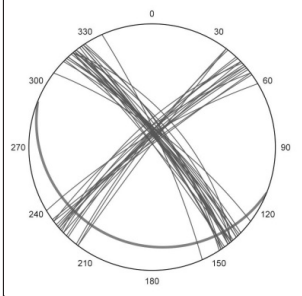	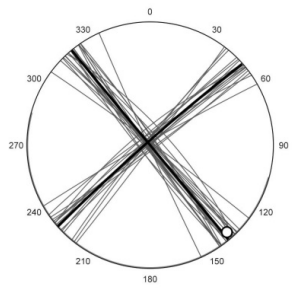	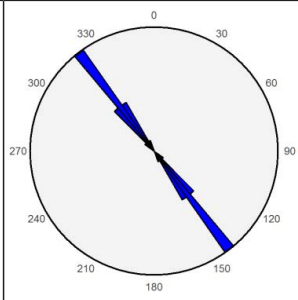	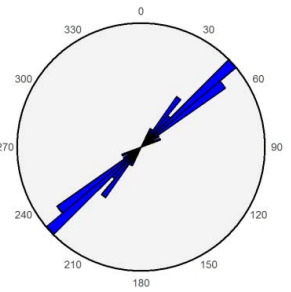
SR2 P2	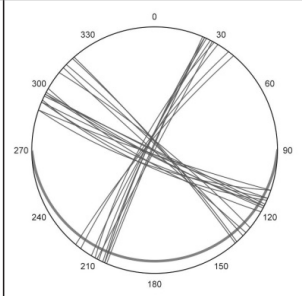	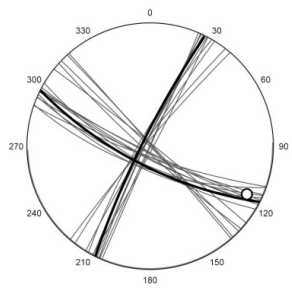	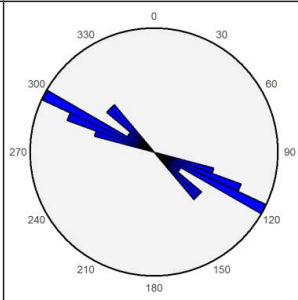	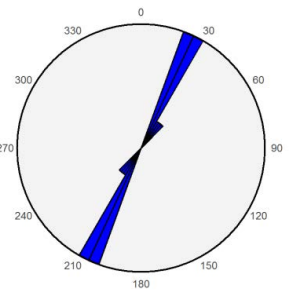
SR3	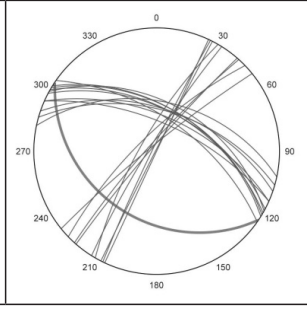	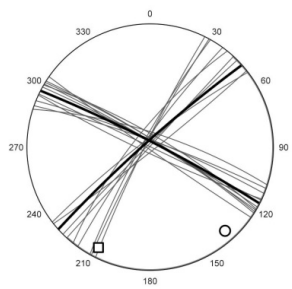	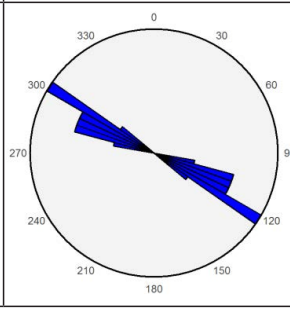	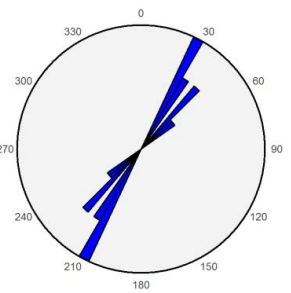

site	present-day orientation	restored to horizontal position	F1 fractures	F2 fractures
SR4	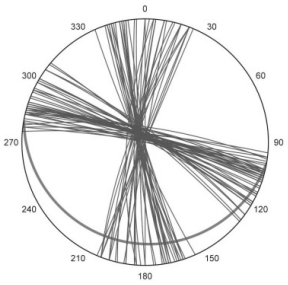	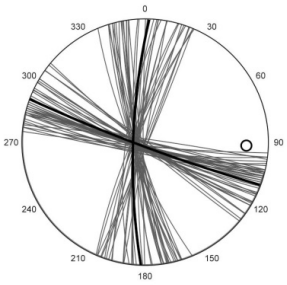	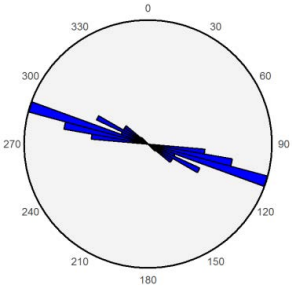	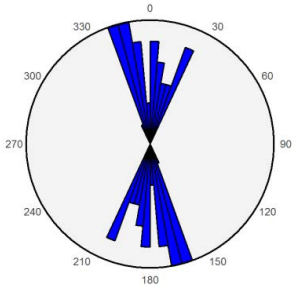
FR1	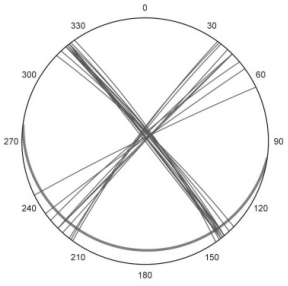	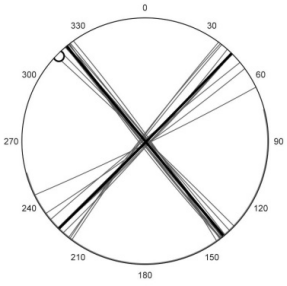	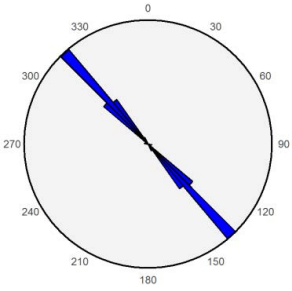	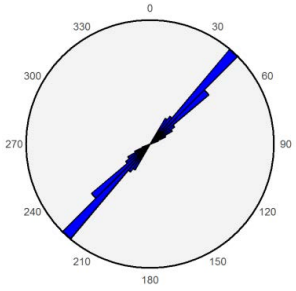
FR2	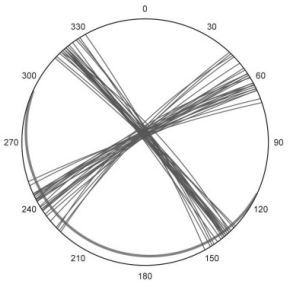	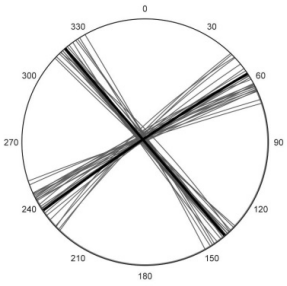	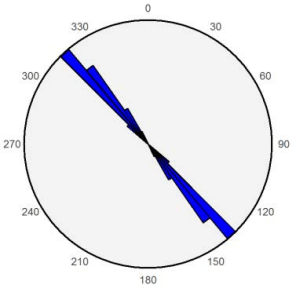	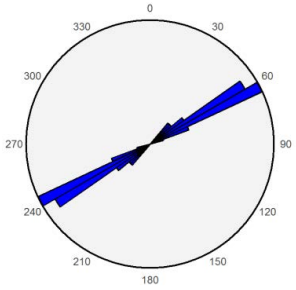
FR3	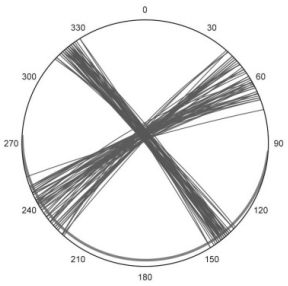	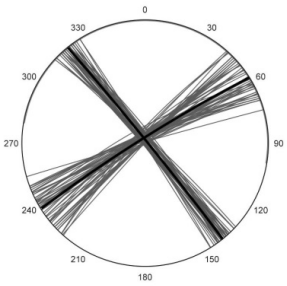	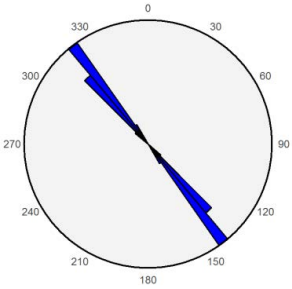	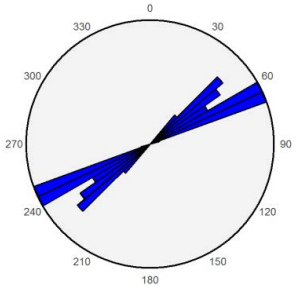
FR4	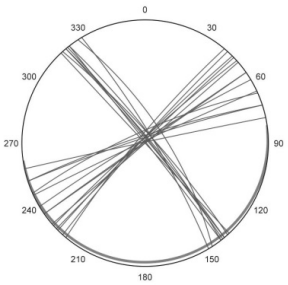	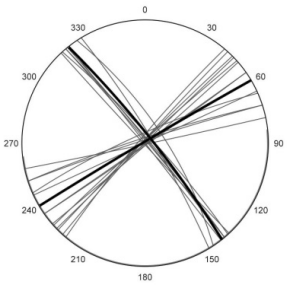	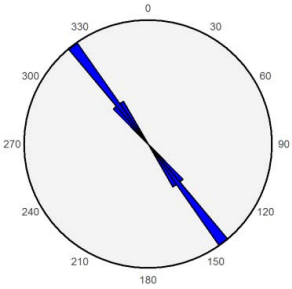	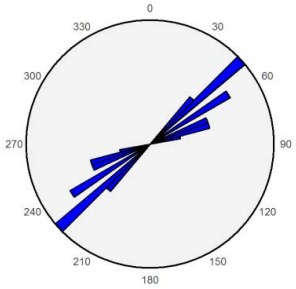
FR5	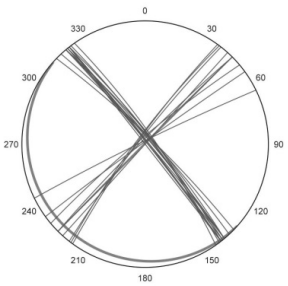	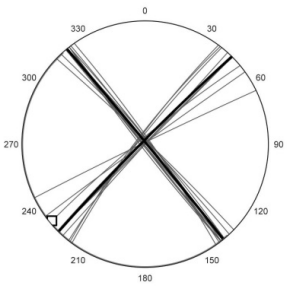	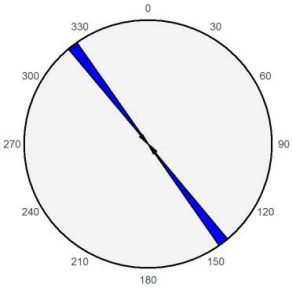	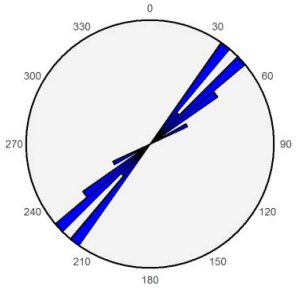

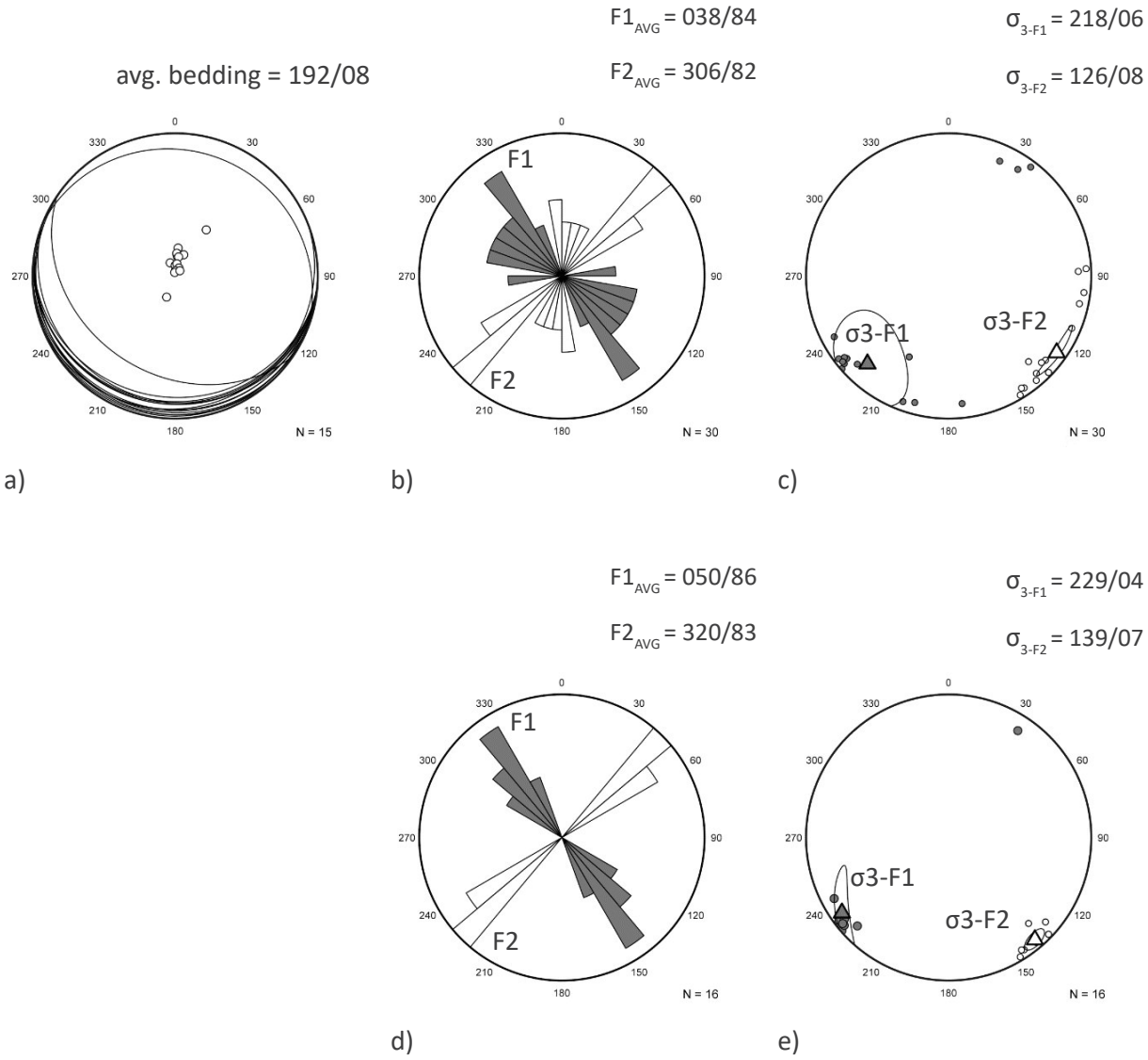

Fig. 4. Summary plots of orientations of investigated structures, averaged for each measurement site. a) Bedding. b) Circular histogram of fracture sets orientations. Bin size is 10°. c) Inferred directions of tensional stress axes from fracture sets F1 in and F2, assuming tension is perpendicular to the plane of average fracture orientation. d) and e): same as in b) and c), but excluding sites SR from the Strunjan structure. See text for discussion.

In few places, weak plumose ornamentations were found on F1 and F2 fracture faces (Fig. 2h), suggesting Mode I opening with horizontal propagation direction. Additionally, up to several mm thick calcite-filled tensional gashes paralleling F1 fractures are occasionally found in sandstone beds (Fig. 2g). We therefore interpret F1 and F2 fractures as tensional joints which originated perpendicular to the axis of minimal stress σ_3.

According to this interpretation, we infer the σ_3 direction at the time of F1 formation to match the normal to average fracture orientation, which implies that F1 joints formed in NE-SW-directed tension (Table 1; Figs. 4c, 4e). This matches well with the known regional extensional episode of probable mid-Miocene age (Vrabec & Fodor, 2006), which was documented in External Dinarides of central Slovenia by fault-slip data inversion (Žibret & Vrabec, 2016).

From the observed field relationships we interpret that F2 fractures postdate the F1 fractures. Inferred σ_3 orientations (Table 1; Figs. 4c, 4e) suggest their origin in NW-SE-oriented tension. We therefore presume that F2 fractures formed in an independent extensional phase concurrently with the NE-SW-striking normal faults that were previously documented both in outcrop scale in the coastal cliff (Vrabec & Rožič, 2014) and in map scale in the interior (Rokava Fault of Placer, 2005).

Table 1. Site coordinates and average orientation of fracture sets for each investigated site.

site	site coordinates		bedding orientation	fracture set F1				fracture set F2				angle between D1 and D2
	ϕ	λ		N	average orientation	dispersion (°)	average pole orientation	N	average orientation	dispersion (°)	average pole orientation	
DR1	45°35′23.8″N	13°42′12.1″E	022/13	73	213/78	2	033/12	88	320/85	2	140/05	70
IR1	45°32′07.4″N	13°37′29.2″E	185/12	47	046/78	3	226/12	26	311/79	11	131/11	87
IR2	45°32′23.0″N	13°37′02.1″E	186/16	30	062/80	4	242/10	29	317/71	7	137/19	79
SR1-1	45°31′59.8″N	13°36′03.7″E	187/11	9	354/79	5	174/11	12	267/86	5	087/04	86
SR1-2	45°31′59.8″N	13°36′03.7″E	184/13	29	015/81	11	195/09	20	277/85	6	097/05	83
SR1-3	45°31′59.8″N	13°36′03.7″E	159/08	13	217/85	19	037/05	23	282/83	39	102/07	65
SR2-1	45°31′59.8″N	13°36′03.7″E	202/13	24	051/79	3	231/09	20	318/81	5	138/09	89
SR2-2	45°31′59.8″N	13°36′03.7″E	180/06	10	204/77	126	024/13	16	293/83	142	113/07	87
SR3	45°32′13.0″N	13°36′07.2″E	214/32	11	026/53	4	206/37	9	313/78	44	133/12	69
SR4	45°32′15.3″N	13°36′15.8″E	190/11	40	020/83	3	200/07	42	268/80	11	088/10	70
FR1	45°31′42.2″N	13°34′27.4″E	188/07	81	049/89	32	229/01	69	314/87	5	134/03	85
FR2	45°31′43.0″N	13°34′25.8″E	205/05	22	050/85	11	230/05	29	326/84	164	146/06	87
FR3	45°31′45.3″N	13°34′15.7″E	184/03	49	053/86	2	233/04	58	327/83	3	147/07	86
FR4	45°31′43.8″N	13°34′22.8″E	172/02	9	052/82	6	232/08	14	329/87	8	149/03	83
FR5	45°31′35.6″N	13°34′40.1″E	222/04	14	051/85	2	231/05	10	314/87	8	134/03	83

Fracture Spacing Index

It is commonly observed that the density, or spacing, of systematic fractures in layered rocks is roughly proportional to layer thickness, but may also be dependent on rock type (e.g. Davis & Reynolds, 1996). In our study area, clearly expressed fractures only occur in sandstone beds, therefore the effect of lithology on their spacing should be negligible. For analysing fracture spacing – layer thickness relationship it is common to use the median of fracture spacing for each measured bed since the frequency distribution of interfracture distances is usually skewed from normal distribution (Narr & Suppe, 1991). A summary of our fracture spacing measurements is presented in Table 2. For each joint set, we then plotted median joint spacing against the respective layer thickness (Fig. 5) to derive fracture spacing index (FSI), which is the slope of the regression line in this plot (Narr & Suppe, 1991). Thus defined, larger FSI values indicate higher joint density.

We find that spacing of joint sets F1 and F2 in Eocene flysch sandstone of the Slovenian coastal area is reasonably-well correlated to bed thickness (Fig. 5). Whereas the recorded range of joint spacing is quite high, the median values tend to stay at the lower end of the range, reflecting that modest joint spacings dominate the frequency distribution. For both joint sets, the dispersion in median joint spacings values appears to be lower for smaller layer thicknesses under 20 cm than for layers between 20 and 35 cm thick. For joint set F1 the derived FSI value is 0.483 with correlation coefficient R^2 of 0.6331. For joint set F2 the FSI value is 0.616 with correlation coefficient R^2 of 0.5035.

We conclude that joint spacing in sets F1 and F2 is reasonably predictable. The joint density may additionally depend on the degree of deformation. We could not conclusively determine this since the total number of measurements was relatively low, therefore FSI determinations for individual structural domains did not yield satisfactory high correlations. Moreover, the structural domains used in this study were defined with respect to the style and amount of shortening deformation, whereas the joints have originated in independent tensional episodes. Joint density is therefore not likely to spatially correlate with shortening domains.

Table 2. Summary statistical data for fracture spacing measurements.

site	bed	bed thickness (cm)	fracture set F1 spacing (cm)					fracture set F2 spacing (cm)				
			median	average	standard deviation	minimum	maximum	median	average	standard deviation	minimum	maximum
SR1	P1	17,0	26,3	28,5	15,4	6,9	64,8	34,3	42,2	30,8	16,1	76,1
SR1	P2	8,5	18,5	19,4	8,6	3,1	35,1	7,1	11,0	8,1	3,8	27,3
SR1	P3	11,1	21,3	23,0	11,4	8,1	52,3	15,9	17,5	8,1	4,2	33,0
SR2	P1	16,2	19,6	21,1	11,9	3,1	47,2	18,2	19,3	8,7	5,2	38,0
SR2	P2	13,0	19,2	25,3	16,5	6,9	62,9	26,0	26,3	15,7	2,5	50,9
SR3	P1	13,0	26,2	21,0	11,2	6,8	32,5	16,0	19,3	9,0	9,5	34,1
SR4	P1	10,0	16,1	11,7	7,7	2,6	21,6	11,2	16,3	4,6	3,9	28,6
SR4	P2	10,2	9,0	8,3	2,3	4,1	12,4	8,4	9,8	3,5	4,9	17,9
IR1	P1	5,0	7,6	7,6	2,5	3,1	12,5	10,2	11,0	5,2	2,9	21,0
IR1	P2	4,6	6,3	7,1	2,6	3,1	12,6	13,2	12,7	3,6	4,9	17,6
IR2	P1	24,0	54,9	58,7	13,6	41,7	81,3	33,2	31,0	6,1	24,0	36,8
IR2	P2	26,4	39,3	33,8	17,5	5,0	60,1	19,8	18,5	7,1	2,7	30,2
FR1	P1	32,0	33,4	36,6	21,1	7,9	89,0	33,6	35,4	10,9	23,4	57,3
FR1	P2	16,0	28,2	29,5	11,4	8,3	59,1	19,3	20,5	8,0	8,6	35,1
FR2	P1	9,0	25,5	25,2	7,4	12,4	39,3	15,0	16,2	6,1	8,2	31,4
FR3	P1	12,0	23,6	22,5	11,2	2,2	47,2	13,4	15,2	6,9	4,5	26,2
FR3	P2	10,5	16,0	17,7	7,7	2,2	47,2	11,2	11,3	5,5	1,8	30,0
FR4	P1	17,7	26,1	25,6	10,5	12,6	47,9	25,9	26,1	4,9	19,7	33,7
FR5	P1	23,2	47,7	47,4	20,5	14,8	81,8	13,3	14,5	6,4	8,8	21,5
DR1	P1	11,5	26,9	27,1	10,0	5,8	55,4	16,7	17,1	7,1	6,1	34,5
DR1	P2	24,8	31,9	36,8	17,7	12,3	74,4	29,0	27,2	8,6	9,6	39,1
DR1	P3	12,2	25,4	23,3	7,0	9,0	34,1	20,0	20,0	8,1	7,6	34,3

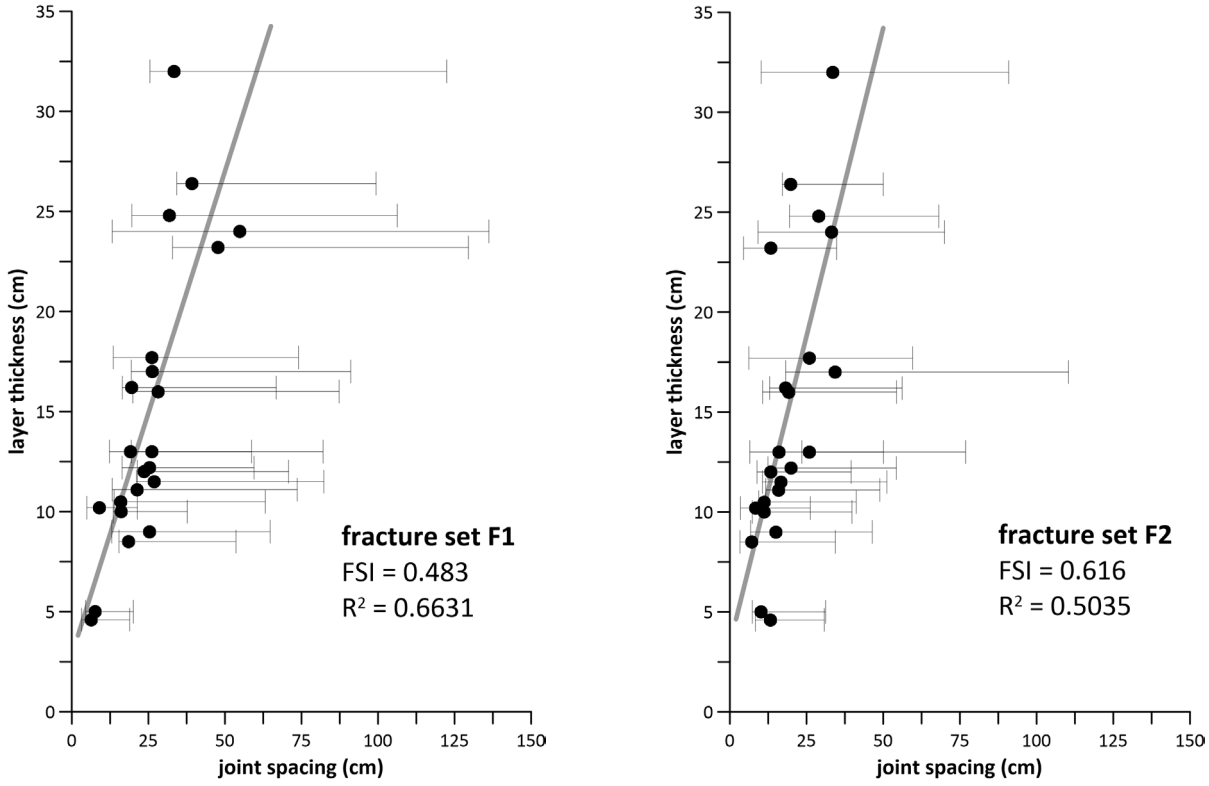

Fig. 5. Fracture spacing index (FSI) determination in Eocene flysch sandstone layers according to Narr & Suppe (1991). Plotted are median fracture spacing distances (black dots) with indicated range of measured spacing values against respective layer thicknesses. FSI value corresponds to the slope of the regression line. a) Fracture set F1; b) fracture set F2.

Discussion and conclusions

The first structural study of systematic fractures in Eocene flysch sandstones in the foreland of the External Dinarides fold-and-thrust belt of the Slovenian coastal area has revealed that the fractures occur in two major sets. The first set F1 comprises NW-SE oriented tensional (Mode I) joints which originated in NE-SW directed tension. This direction is roughly parallel to the shortening direction implied from the orientation of thrusts and folds in the coastal area, therefore we assume that extension is independent of thrusting (i.e., it does not represent shortening-perpendicular extension which is relatively common in thrustbelts). We correlate the origin of F1 joints to the well-documented regional extensional episode, which postdates Dinaric thrusting (see Žibret & Vrabec, 2016 for outcrop-scale and map-scale evidence). In the Slovenian coastal area however, the F1 joints and associated tensional gashes clearly formed when bedding was still in horizontal orientation. This implies that Dinaric shortenting did not significantly (if at all) affect the Slovenian coastal area. The thrusting and folding which tilted the beds must therefore be both post-Dinaric and younger than NE-SW extension which is presumably of mid-Miocene age (Vrabec & Fodor, 2006). This conclusion corroborates well with the early interpretation of Placer (2007) that the coastal shortening deformation reflects young underthrusting of the Adria microplate which is independent of and subsequent to Dinaric thrusting. Our tentative chronology constrains the start of underthrusting to Late Miocene, as already presumed by Placer (2007), or even to Miocene – Pliocene transition.

Fractures of the second set F2 are NE-SW-oriented and intersect F1 joints in a nearly perpendicular orientation, with the average intersection angle of 80°. In our interpretation F2 fractures are younger and probably originated as tensional joints in a distinct extensional episode with NW-SE oriented tension, which was so far not documented in other parts of Slovenia. The relative timing of this second extension is not clear as the available data is contradictory. The orientation of F2 joints and of mesoscopic normal faults originating in the same extensional regime (Vrabec & Rožič, 2014) with respect to bedding implies that this extension also predates the tilting of the beds and is therefore probably older than shortening. On the other hand, the map-scale Rokava Fault, also implying NW-SE extension, is interpreted by Placer (2005) to cut and postdate the Buzet Thrust, a major thrust structure of the post-Dinaric coastal belt, but it apparently does not cut other thrusts in the hinterland of Buzet Thrust. Finally, geodetic data from GNSS campaigns convincingly demonstrate ongoing NNW-SSE-directed shortening in the area with no indications for contemporaneous NW-SE extension (Weber et al., 2010).

Our study shows that the orientations of F1 and F2 fractures remain reasonably constant along the entire transect crossing all major structural domains of the coastal belt. This implies that the fracture orientations probably reflect regional-scale paleostress fields and are largely independent of local influences. The only significant deviations occur in the Strunjan structure, which is a frontal deformed area with reverse faults and asymmetric folds verging in the opposite direction to the overall SW-ward vergence of the coastal area structures.

We also investigated the fracture spacing with respect to layer thickness to determine the fracture spacing index (FSI), and found that the correlation is reasonably good. The systematic relationships of fracture orientations and their spacing with respect to bedding thickness established in this study may be utilized in future engineering and resource utilization projects.

References

Busetti, M., Volpi, V., Nicolich, R., Barison, E., Romeo, R., Baradello, L., Brancatelli, G., Giustiniani, M., Marchi, M., Zanolla, C., Wardell, N., Nieto, D. & Ramella, R. 2010: Dinaric tectonic features in the Gulf of Trieste (Northern Adriatic Sea). Bolletino di Geofisica Teorica e Applicata, 51: 117–128.

Carulli, G.B. 2011: Structural model of the Trieste Gulf: A proposal. Journal of Geodynamics, 51/2-3: 156–165, doi:10.1016/j.jog.2010.05.004.

Davis, G.H. & Reynolds, S.J. 1996: Structural Geology of Rocks and Regions. John Wiley & Sons, New York: 776 p.

Moulin, A., Benedetti, L., Rizza, M., Jamšek Rupnik, P., Gosar, A., Bourlès, D., Keddadouche, K., Aumaître, G., Arnold, M., Guillou, V. & Ritz, J-F. 2016: The Dinaric fault system: Large-scale structure, rates of slip, and Plio-Pleistocene evolution of the transpressive northeastern boundary of the

Adria microplate. Tectonics, 35: 2258–2292, doi:10.1002/2016TC004188.

Narr, W. & Suppe, J. 1991: Joint spacing in sedimentary rocks. Journal of Structural Geology, 13/9: 1017-1048, doi:10.1016/0191-8141(91)90055-N.

Otoničar, B. 2007: Upper Cretaceous to Paleogene forbulge unconformity associated with foreland basin evolution (Kras, Matarsko podolje and Istria; SW Slovenia and NW Croatia). Acta Carsologica, 30: 101-120, doi:10.3986/ac.v36i1.213

Pavšič, J. & Peckmann, J. 1996: Stratigraphy and sedimentology of the Piran flysch area (Slovenia). Annales: Seria Historia Naturalis, 9: 123–138.

Placer, L. 2005: Strukturne posebnosti severne Istre. Geologija, 48/2: 245-251, doi:10.5474/geologija.2005.020.

Placer, L. 2007: Kraški rob - Geološki prerez vzdolž AC Kozina – Koper. Geologija, 50/1: 29-44, doi:10.5474/geologija.2007.003.

Placer, L. 2008: Osnove tektonske razčlenitve Slovenije. Geologija, 51/2: 205-217, doi:10.5474/geologija.2008.021.

Placer, L. 2015: Simplified structural map of Kras Kras (Slovene), Carso (Italian) = Geographical unit. Geologija, 58/1: 89-93, doi:10.5474/geologija.2015.008.

Placer, L., Košir, A., Popit, T., Šmuc, A. & Juvan, G., 2004: Buzetski narivni prelom v Istri in inverzne karbonatne megaplasti v eocenskem flišu v dolini Dragonje. Geologija, 47/2: 193-198, doi:10.5474/geologija.2004.015.

Placer, L., Celarc, B. & Vrabec, M. 2010: Osnove razumevanja tektonske zgradbe NW Dinaridov in polotoka Istre. Geologija, 53/1: 55-86, doi:10.5474/geologija.2010.005.

Vollmer, F.W. 2015: Orient 3: A new integrated software program for orientation data analysis, kinematic analysis, spherical projections, and Schmidt plots. Geological Society of America Abstracts with Programs, 47: 49.

Vrabec, M. & Fodor, L. 2006: Late Cenozoic Tectonics of Slovenia: Structural Styles at the Northeastern Corner of the Adriatic Microplate. In: Pinter, N., Grenerczy, G., Weber, J., Stein, S. & Medak, D. (eds.): The Adria Microplate: GPS Geodesy, Tectonics and Hazards, NATO Science Series, IV, Earth and Environmental Sciences, 61, 151–168, doi:10.1007/1-4020-4235-3_10.

Vrabec, M., Šmuc, A., Pleničar, M. & Buser, S. 2009: Geološki razvoj Slovenije – povzetek. In: Pleničar, M., Ogorelec, B. & Novak, M. (eds.): Geologija Slovenije, Geološki zavod Slovenije, Ljubljana: 29-33.

Vrabec, M. & Rožič, B. 2014: Strukturne in sedimentološke posebnosti obalnih klifov. In: Rožič, B., Verbovšek, T. & Vrabec, M. (eds.): 4. slovenski geološki kongres, Ankaran, 8.-10. oktober 2014. Povzetki in ekskurzije, Naravoslovnotehniška fakulteta, Ljubljana: 84-91.

Vrabec, M., Busetti, M., Zgur, F., Facchin, L., Pelos, C., Romeo, R., Sormani, L., Slavec, P., Tomini, I., Visnovic, G. & Žerjal, A. 2014: Refleksijske seizmične raziskave v slovenskem morju SLOMARTEC 2013. In: Kuhar, M., Čop, R., Gosar, A., Kobold, M., Kralj, P., Malačič, V., Rakovec, J., Skok, G., Stopar, B. & Vreča, P. (eds.): Raziskave s področja geodezije in geofizike 2013. University of Ljubljana, Faculty of Civil and Geodetic Engineering, Ljubljana: 97-101.

Weber, J., Vrabec, M., Pavlovčič-Prešeren, P., Dixon, T., Jiang, Y. & Stopar, B. 2010: GPS-derived motion of the Adriatic microplate from Istria Peninsula and Po Plain sites, and geodynamic implications. Tectonophysics, 483: 214-222, doi:10.1016/j.tecto.2009.09.001.

Žibret, L. & Vrabec, M. 2016: Palaeostress and kinematic evolution of the orogen-parallel NW-SE striking faults in the NW External Dinarides of Slovenia unraveled by mesoscale fault-slip data analysis. Geologia Croatica, 69/3: 295-305, doi:10.4154/gc.2016.30.